NIH Public Access
Author Manuscript
Biochemistry. Author manuscript; available in PMC 2013 January 31.

Published in final edited form as:
Biochemistry. 2012 January 31; 51(4): 836–847. doi:10.1021/bi201772m.

Mapping general anesthetic binding site(s) in human α1β3 γ-aminobutyric acid type A receptors with [^{3}H]TDBzl-etomidate, a photoreactive etomidate analog†

David C. Chiara[‡,‖], **Zuzana Dostalova**[⊥,‖], **Selwyn S. Jayakar**[‡], **Xiaojuan Zhou**[⊥], **Keith W. Miller**[§,⊥], and **Jonathan B. Cohen**[‡,*]

[‡]Department of Neurobiology, Harvard Medical School, Boston, Massachusetts 02115

[§]Department of Biological Chemistry and Molecular Pharmacology, Harvard Medical School, Boston, Massachusetts 02115

[⊥]Department of Anesthesia, Critical Care, and Pain Medicine, Massachusetts General Hospital, Boston, Massachusetts 02114.

Abstract

The γ-aminobutyric acid type-A receptor ($GABA_AR$) is a target for general anesthetics of diverse chemical structures, which act as positive allosteric modulators at clinical doses. Previously, in a heterogeneous mixture of $GABA_ARs$ purified from bovine brain, [^{3}H]azietomidate photolabeling of αMet-236 and βMet-286 in the αM1 and βM3 transmembrane helices identified an etomidate binding site in the $GABA_AR$ transmembrane domain at the interface between the β and α subunits. To further define $GABA_AR$ etomidate binding sites, we now use [^{3}H]TDBzl-etomidate, an aryl diazirine with broader amino acid side-chain reactivity than azietomidate, to photolabel purified human FLAG-α1β3 $GABA_ARs$ and obtain a more extensive identification of photolabeled $GABA_AR$ amino acids. [^{3}H]TDBzl-etomidate photolabeled in an etomidate-inhibitable manner β3Val-290, in the β3M3 transmembrane helix, as well as α1Met-236 in α1M1, a residue photolabeled by [^{3}H]azietomidate, while no photolabeling was detected of amino acids in the αM2 or βM2 helices that also border the etomidate binding site. The location of these photolabeled amino acids in $GABA_AR$ homology models derived from the recently solved structures of prokaryote (GLIC) or invertebrate (GluCl) homologs and the results of computational docking studies predict the orientation of [^{3}H]TDBzl-etomidate bound in that site and the other amino acids contributing to this $GABA_AR$ intersubunit etomidate binding site. Etomidate-inhibitable photolabeling of β3Met-227 in βM1 by [^{3}H]TDBzl-etomidate and [^{3}H]azietomidate also provides evidence of an homologous etomidate binding site at the β3-β3 subunit interface in the α1β3 $GABA_AR$.

†This research was supported by a grant from the National Institutes of Health (GM-58448).

*To whom correspondence should be addressed: Phone: (617) 432-1728, Fax: (617) 432-1639. jonathan_cohen@hms.harvard.edu..
‖These authors contributed equally to this work.

SUPPORTING INFORMATION AVAILABLE: Supplemental Methods concerning the docking calculations and ten figures: (1) Amino acid sequence alignments used to create the $GABA_AR$ homology models; (2) Helical wheel representations of the transmembrane domain β3-α1 interface in the 3 $GABA_AR$ homology models; (3) Comparison of the $GABA_AR$ transmembrane domain β3-α1 interface in the three $GABA_AR$ homology models; (4) $GABA_AR$ amino acids contributing to the TDBzl-etomidate pocket at the β3-α1 interface (stereo representation); (5-7) Stereo images of TDBzl-etomidate docked into: (5) a β3-α1 interface in homology models derived from the structures of GluCl and GLIC; (6) a pocket at the $GABA_AR$ β3-β3 interface; (7) the pockets within the $GABA_AR$ α and β subunit helix bundles; (8) and (9) rpHPLC fractionations of EndoGlu-C (8) and trypsin/EndoLys-C (9) digests of [^{3}H]azietomidate or [^{3}H]TDBzl-etomidate photolabeled $GABA_AR$ subunits; (10) Sequence analysis of [^{3}H]TDBzl-etomidate photoincorporation in β3M2. Supplemental materials may be accessed free of charge online at http://pubs.acs.org.

CONFLICT OF INTEREST DISCLOSURE: The authors declare no competing financial interest.

NIH-PA Author Manuscript
NIH-PA Author Manuscript
NIH-PA Author Manuscript

NIH-PA Author Manuscript

NIH-PA Author Manuscript

NIH-PA Author Manuscript

General anesthetics have been employed to relieve surgical suffering for some 165 years, but their sites of action have proven hard to define. Inhaled anesthetics act at relatively high concentrations (~10^{-4} M) and their pharmacologies are complex and multifactorial. In contrast, some intravenous agents act at sufficiently low concentrations (~10^{-6} M) to exhibit relatively specific pharmacology (1,2). Prime amongst these is etomidate, an agent that acts in the low micromolar range (3). *R*-etomidate is ten times more potent than *S*-etomidate in anesthetic potency, a degree of enantioselectivity rare for a general anesthetic, and physiological studies demonstrate the same enantioselectivity for the γ-aminobutyric acid type A receptors ($GABA_AR$) (4). At low concentrations etomidate enhances currents elicited by subsaturating concentrations of GABA, whereas at higher concentrations, it can elicit currents in the absence of GABA. These actions are consistent with a model where low occupancy of two equivalent etomidate binding sites enhances GABA-elicited currents and high occupancy induces gating independent of the GABA site (5).

$GABA_ARs$ belong to the Cys-loop superfamily of receptors, each consisting of five identical or homologous subunits arranged pseudo-symmetrically around a central ion pore (6,7). The transmembrane domain of each subunit is made up of a loose bundle of 4 α helices (M1-M4), with amino acids on one face of each M2 helix forming the lumen of the ion channel. Etomidate's action depends strongly on the subunit composition of $GABA_ARs$, with the presence of β2 or β3 subunits necessary for high sensitivity (8). Based on studies with chimeric β subunits, mice were created containing a point mutation (N265M) in the M2 helix of the β3 subunit, and etomidate's potency was shown to be strongly attenuated (9,10).

The latter studies define one molecular target of etomidate's *in vivo* action, those $GABA_ARs$ that contain β3 subunits, but they do not determine whether the point mutation modifies the etomidate binding site or alters anesthetic potency allosterically. In the absence of high resolution structures, one strategy for locating the binding site is to develop photoactivatable general anesthetics that are stable under normal conditions, but insert covalently into their binding site when activated by UV irradiation. The first such etomidate derivative, azietomidate, mimicked etomidate faithfully (11). It was equipotent as a general anesthetic and a $GABA_AR$ potentiator, and it exhibited similar enantioselectivity. Furthermore, introduction of the β3N265M point mutation into mice attenuated azietomidate's general anesthetic potency (12). These studies strongly suggest that etomidate and azietomidate act at the same site.

Employing [^{3}H]azietomidate to photolabel a heterogeneous population of $GABA_ARs$ purified from bovine brain, etomidate-inhibitable photoincorporation was found in two residues, Met-236 (α1 numbering) within an α subunit M1 helix and Met-286 in a β subunit M3 helix (13). Based on a $GABA_AR$ homology model derived from the structure of the *Torpedo* nicotinic acetylcholine receptor (nAChR) (14), it was hypothesized (13) that etomidate bound in the transmembrane domain at a pocket between the β and α subunits of a single $GABA_A$ receptor, the interface between subunits that also contains the GABA binding site in the extracellular domain. Although this was the first direct identification of amino acids contributing directly to a $GABA_AR$ anesthetic binding site, definition of the structure of the etomidate binding site was limited by several factors: (i) The diversity of $GABA_AR$ subunit combinations purified on the benzodiazepine affinity column and the high degree sequence identity in the regions of primary structure containing the photolabeled amino acids precluded the identification of the photolabeled α and β subunit subtypes. (ii) This $GABA_AR$ heterogeneity, in conjunction with the limited quantities of $GABA_AR$ that can be purified from brain and the fact that photoactivated azietomidate can react only with nucleophilic, but not aliphatic, amino acid side chains (15,13,16), made difficult the identification of photolabeled amino acids in other regions of primary structure. (iii) The validity was uncertain of $GABA_AR$ homology models derived from *Torpedo* nAChR

NIH-PA Author Manuscript

NIH-PA Author Manuscript

NIH-PA Author Manuscript

structure, the only structure then available, but whose subunits lack sequence and length conservation with $GABA_AR$ subunits in the M3 region. In other such homology models (17,18), one or both of the photolabeled amino acids were not located at the β-α interface.

To circumvent these limitations, in this work we photolabel purified human FLAG-α1/β3 $GABA_ARs$ (19) with a novel photoreactive etomidate analog, [^{3}H]TDBzl-etomidate (Figure 1), and we interpret the results by use of $GABA_AR$ homology models based upon the recently solved structures of prokaryote (GLIC (20)) and invertebrate (GluCl (21)) homologs that have a high degree of amino acid sequence conservation with the $GABA_AR$ M3 and M4 helices. TDBzl-etomidate acts as a positive modulator of the $GABA_AR$ at concentrations producing anesthesia (22), and when photoactivated it forms a carbene that can react with most amino acid side chains, including aliphatics (23). This broad side chain reactivity makes [^{3}H]TDBzl-etomidate a favorable probe to determine the extent of the β3-α1 subunit interface contributing to that etomidate binding site and to determine whether etomidate binds to additional sites in the $GABA_AR$. For comparison with photolabeling results obtained with the bovine brain αβγ $GABA_ARs$, we also photolabel the FLAG-α1/β3 $GABA_AR$ with [^{3}H]azietomidate.

EXPERIMENTAL PROCEDURES

Materials

[^{3}H]muscimol (3-hydroxy-5-aminomethylisoxazole, [methylene-^{3}H(N)], 22.5 Ci/mmol) was from Perkin Elmer (Waltham, MA). n-Dodecyl-β-D-maltopyranoside, sodium cholate, and 3-[(3-cholamidopropyl)dimethylammonio]-1-propanesulfonate (CHAPS) were from Anatrace-Affymetrix (Anagrade quality). Anti-FLAG M2 affinity gel, FLAG peptide (DYKDDDDK), GABA (γ-aminobutyric acid), polyethylene glycol, γ-globulins from bovine blood, soybean asolectin, and 3-bromo-3-methyl-2-(2-nitrophenylthio)-3H-indole (BNPS-skatol, B4651) were from Sigma–Aldrich. [^{3}H]Azietomidate (12 Ci/mmol) and [^{3}H]TDBzl-etomidate (16 Ci/mmol) were synthesized as described (11,22). *R*-Etomidate was from Organon Laboratories. *S. aureus* Glutamic-C endopeptidase (EndoGlu-C) was from Princeton Separations (Adelphia, NJ), and *Lysobacter enzymogenes* Lysine-C endopeptidase (EndoLys-C) was from Princeton Separations and from Roche Applied Science. Trypsin-TPCK treated was obtained from Worthington Biochemical Corp. *o*-Phthalaldehyde (OPA) was purchased from Alfa Aesar.

Preparation of α1β3 $GABA_A$ receptors

α1β3 $GABA_ARs$ with a FLAG epitope at the N-terminus of the α1 subunit were expressed in a tetracycline-inducible, stably transfected HEK293S cell line as described (19) and purified using a modification of that published procedure. Briefly, membranes from 40-60 15–cm plates (1 mg protein/mL; 6-10 nmol of [^{3}H]muscimol binding sites) were solubilized overnight at 4 °C in ~ 300 mL purification buffer (50 mM Tris-HCl (pH 7.4), 150 mM NaCl, 2 mM $CaCl_2$, 5 mM KCl, 5 mM $MgCl_2$, 4 mM EDTA, 20% glycerol, 10 μg/mL each of pepstatin, chymostatin, and leupeptin, 2 μg/mL aprotinin, and 1 mM phenylmethylsulfonyl fluoride) supplemented with 2.5 mM n-dodecyl-β-D-maltopyranoside and then centrifuged at 100,000 × g for 30 min. Aliquots of supernatant (60-80 mL) were incubated for 2 h at 4 °C with 2 mL of Anti-FLAG M2 affinity resin (capacity ~2 nmol [^{3}H]muscimol binding sites) that had been pretreated with poly-D-lysine HBr as described (19), which was then transferred to five Bio-Rad Econo columns. The columns at 4 °C were washed with 6 bed volumes of lipid-exchange buffer (purification buffer supplemented with 17 mM cholate and 8.5mM asolectin), agitated for 30 min with 5 volumes of lipid-exchange buffer, washed with 2 volumes of lipid-exchange buffer, and then washed with 3 volumes of wash buffer (purification buffer supplemented with 11.5 mM cholate and 0.86 mM

NIH-PA Author Manuscript

NIH-PA Author Manuscript

NIH-PA Author Manuscript

asolectin). Receptors were eluted by incubating the resin for 5-10 min with 5-6 successive batches (0.5 bed volume each) of elution buffer (wash buffer supplemented with 0.1 mM FLAG peptide). The parallel elutions from each of the columns were pooled, aliquoted, frozen and stored at –80 °C. Aliquots from each pooled elution were characterized by SDS-PAGE for purity and by [^{3}H]muscimol binding for receptor concentration and anesthetic modulation. Individual purifications started from membranes containing 11-12 nmol of [^{3}H]muscimol binding sites (2 pmol/mg protein) and typically resulted in ~ 1.5 nmol of purified receptor (50-60 nM binding sites) in 15-25 mL of elution buffer.

Radioligand binding assays

[^{3}H]muscimol binding to purified $GABA_AR$ was measured by filtration after receptor precipitation with polyethylene glycol (13). To measure the total number of sites, the sample tube contained 12 nM [^{3}H]muscimol (final concentration) and 35-70 μL of purified $GABA_AR$, diluted to 3.6 mL in assay buffer (200 mM KCl, 10 mM phosphate buffer (pH 7.4), 1 mM EDTA, and 5 mM CHAPS). Because of non-specific binding, a subsaturating concentration of [^{3}H]muscimol was used, and the number of sites was calculated from the dissociation constant (K_D = 10 nM) as described (19). To measure anesthetic modulation, the sample (3.6 mL in assay buffer) contained 350-1050 μL purified $GABA_AR$, 1 nM [^{3}H]muscimol (final concentration), and anesthetic. At the start of the incubation, half of each sample was used to measure non-specific binding, which was determined by addition of 1 mM GABA (final concentration). Samples were equilibrated at 4°C for 45 min in the absence or presence of anesthetics, and then 1.4 mL of polyethylene glycol (15.5 % final concentration) and γ-globulins (0.1 % final concentration) were added to precipitate the $GABA_AR$. Fifteen minutes after this addition, three aliquots of 0.9 mL for each condition were filtered on glass fiber filters (Whatman GF/B) that had been pretreated for 1 h in 0.5% w/v poly(ethyleneimine). Filters were washed under vacuum with 7 mL of ice cold assay buffer supplemented with polyethylene glycol (7% final concentration), and ^{3}H retention on the dried filters was determined by liquid scintillation counting. For anesthetic titrations, total and non-specific binding were determined at each anesthetic concentration, with the total and non-specific control binding (no added anesthetic) determined in quadruplicate. Specific binding (total – nonspecific) was calculated from the means of the triplicate determinations with error propagation using their standard deviations. The potentiation of specific [^{3}H]muscimol binding (P, as % control) at anesthetic concentration x was fit to equation 1:

$$P(x) = (P_{max} - 100) / (1 + EC_{50}/x) + 100, \quad \text{Eq. 1}$$

where P_{max} is the maximal potentiation and EC_{50}, the anesthetic concentration causing half-maximal potentiation.

Photoaffinity labeling

Aliquots of purified $GABA_AR$ in elution buffer (~65 pmol [^{3}H]muscimol sites/mL) were used for analytical (3-15 pmol/condition) and preparative (115-130 pmol/condition) scale photolabeling. Appropriate amounts of [^{3}H]azi-etomidate or [^{3}H]TDBzletomidate were transferred to glass tubes, and solvent (methanol) was evaporated under an argon stream. Freshly thawed $GABA_AR$ in elution buffer was then added to the tube, and the dried [^{3}H]photoetomidate was resuspended with intermittent gentle vortexing for a minimum of 30 min to a final concentration of 0.5 - 10 μM. Aliquots were incubated for 30 min with 1 mM GABA (included to avoid potential photolabeling of the GABA binding sites and to stabilize the $GABA_AR$ in a conformation with high affinity for etomidate and its analogs) ± 100 μM etomidate. The samples were then placed in individual wells of a 96 well plastic microtiter plate (Falcon #353911, analytical photolabeling) or in a plastic 3.5 cm diameter

NIH-PA Author Manuscript

NIH-PA Author Manuscript

NIH-PA Author Manuscript

petri dish (Falcon #3001, preparative labeling) and irradiated on ice for 30 min at a distance of 2 cm with a 365 nm lamp (Spectroline Model EN-16, Spectronics, Westbury, N.Y.). After irradiation, the samples were mixed with an equal volume of electrophoresis sample buffer (freshly mixed 1 part 2-mercaptoethanol with 9 parts of a solution composed of 40 % sucrose, 10 % SDS, 2 % glycerol, 0.0125 % bromophenol blue, and 0.3 M Tris, pH 6.8), incubated for 15 min, and fractionated by SDS-PAGE.

SDS-PAGE

For analytical scale photolabeling, the ^{3}H incorporation into individual subunits was quantified by liquid scintillation counting of excised gel bands that had been hydrated in 200 μL deionized water and incubated in gel cocktail [5 mL of freshly mixed 90 % Ecoscint A (National Diagnostics) + 10 % TS-2 tissue solubilizer (Research Products, Inc.)] for 3 days.

Because the preparative photolabeling of $GABA_AR$ in detergent resulted in volumes of 4-5 mL of receptor in sample buffer containing as much as ~ 1 mCi ^{3}H, electrophoresis conditions were optimized to handle the large sample volumes and to allow the containment and removal of the unincorporated ^{3}H directly from the gel prior to staining. For this purpose, 1.5 mm thick Laemmli slab gels (8% acrylamide, 0.32% bis-acrylamide resolving gel) were poured that were 16 cm long and 14 cm wide, with a 3 cm stacker layer (4% acrylamide, 0.16% bis) and wells that were 5 cm deep and 12 cm wide. The samples were electrophoresed overnight at 12 mA constant current, and electrophoresis was stopped when the dye front was 4-5 cm from the bottom end of the gel. Prior to staining, the region of the gel below the dye front was excised, safely removing the majority of the unincorporated ^{3}H. Gels were stained with Coomassie Blue stain. Gel bands of interest from preparative labelings were excised and eluted in 12 mL elution buffer (100 mM NH_4HCO_3, 0.1% SDS, & 2.5 mM dithiothreitol, pH 8.4, 3 days with constant rocking). Eluates were filtered, concentrated to < 400 μL, acetone precipitated (75% acetone, > 4 hr, -20 °C), and resuspended in 100 μL of digestion buffer [15 mM Tris, 500 μM EDTA, & 0.1% SDS, pH 8.5].

Chemical and enzymatic fragmentation

Proteases were suspended in water immediately before use. Samples were digested at 25 °C with 0.5 U of EndoLys-C (Roche) for two weeks or for 2-3 days with 2.5 μg of EndoLys-C (Princeton Separations) or 5 μg of EndoGlu-C. For digestion with trypsin, samples were first diluted 5-fold with 0.5 % Genapol C-100 (Calbiochem) in 50 mM NH_4HCO_3, pH 7.0, then 1/9 volume containing 10-20 μg of trypsin in 20 mM $CaCl_2$ was added (2 mM $CaCl_2$ final concentration). Chemical cleavage at Trp residues of protein on PVDF filters was achieved using BNPS-skatol as described (24), except that after precipitation of the excess BNPS-skatol, the digestion solution was loaded onto a Prosorb filter for sequencing.

Reversed-phase HPLC and Sequence Analysis

Digested samples were fractionated by rpHPLC as described (13). HPLC fractions of interest were slowly drop-loaded onto glass fiber filters (Applied Biosystems, AB #401111) at 45 °C until all solvent was evaporated. Prior to sequencing, filters were treated with 15 μL of Biobrene Plus (Applied Biosystems #400385). Sequence analysis of intact subunit samples containing SDS were loaded onto Prosorb PVDF filters (AB # 402052) following the Prosorb loading directions. Protein sequence analysis was performed on a Procise 492 protein sequencer (Applied Biosystems) set up to analyze 2/3 of the material from each cycle of Edman degradation for amino acid quantification while collecting the other 1/3 for ^{3}H determination by scintillation counting. Quantification of PTH-amino acids was determined from peak heights, and initial peptide amounts (I_0) and repetitive yields (R) were determined by fitting the background-subtracted pmol for a sequence to equation 2:

NIH-PA Author Manuscript

NIH-PA Author Manuscript

NIH-PA Author Manuscript

$$I_x = I_0 \times R^x \quad \text{Eq. 2}$$

where I_x is the pmol of the residue detected in cycle x. Values for the amino acids Cys, Trp, Ser, and His were excluded from the fits due to known difficulties with their identification or quantification. The specific incorporation (SI, in cpm/pmol) at a single residue was determined by equation 3:

$$SI = 2 \times (cpm_x - cpm_{(x-1)}) / I_x \quad \text{Eq. 3}$$

where cpm_x was the cpm of ^{3}H in cycle x and I_x was calculated from eq. 2. In this equation, $cpm_{(x-1)}$ was used to estimate the background release of ^{3}H.

For some sequences in which a proline residue was encountered prior to the site of labeling, the sequencing filter was treated with OPA (15 μL of the solution: 4 mg OPA / 2 mL acetonitrile / 10 μL β-mercaptoethanol) at the beginning of the proline-containing cycle to block further sequencing of contaminating peptides that do not contain a proline in that cycle, thereby confirming that any subsequently detected peak of ^{3}H release originated from the proline-containing peptide (25,26).

Molecular modeling

Based upon previous studies of the subunit composition of expressed αβ $GABA_A$Rs (27,28), homology models with a subunit ordering β3α1β3α1β3 were constructed using the Discovery Studio (Accelrys, Inc.) software package from the recent crystal structures of two detergent-purified, homopentameric ligand-gated ion channels: GLIC, a proton-gated channel from the prokaryote *Gloeobacter violaceus*, crystallized at pH 4 in the presence of the general anesthetic propofol (PDB:3P50) (20), and GluCl, a glutamate-gated chloride channelfrom *Caenorhabditis elegans*, crystallized at pH 4.5 in the presence of the allosteric activator ivermectin and glutamate (PDB code 3RIF) (21). The high degree of amino acid sequence conservation between the $GABA_A$R subunit M3 and M4 helices and those of GLIC and GluCl, but not with those of the nAChR subunits, allows a more confident alignment of those $GABA_A$R regions in the homology models based upon the GLIC or GluCl structures than upon the moderate resolution cryoelectron microscopy structure of the *Torpedo* nAChR in its native membrane environment (PDB code 2BG9) (14) that we used previously to create a model of the αβγ $GABA_A$R (13) (see Supp. Fig. S1 for the M1-M4 alignments used for our models).

When the transmembrane helices are depicted in helical wheel diagrams (Supp. Fig. S2), the identities of the amino acids of βM3 and αM1 contributing to the β3-α1 subunit interface are the same in the models based upon GLIC and GluCl, and differ in location from the model based upon the nAChR structure only by counter-clockwise (looking down the channel) rotations of amino acids in αM1 and in both M2 helices by ~40° and 20°, respectively, and by a translation of ~one helical turn down in M3. Thus, in the GLIC/GluCl models βMet-286 of βM3 is in register with αLeu-232 in αM1, while in the nAChR-derived model βMet-286 is in register with αIle-228 (Supp. Fig. S3). All models are generally consistent with experimental studies positioning αMet-236 and βMet-286 at the β-α interface, based upon the formation of intersubunit disulfide cross-links between βM286C or βF289C and cysteines substituted in αM1 (29). As noted (21), compared to the GLIC structure there is an increased distance in the GluCl structure between the M3 and M1 helices at that interface where the allosteric activator ivermectin is bound.

CDocker (30), a CHARMm-based molecular dynamics simulated annealing program, was used to dock drugs into potential binding pockets in the αβ $GABA_A$R transmembrane

NIH-PA Author Manuscript

NIH-PA Author Manuscript

NIH-PA Author Manuscript

domain (β3-α1 or β3-β3 interfaces, the α1 and β3 subunit helix bundles, and the ion channel) in the homology models based upon the GLIC and the GluCl structures. Details about the parameters used for docking are presented in Supplemental Methods. The predicted binding site for TDBzl-etomidate at the β3-α1 interface is presented in Figure 8 and in stereo representation in Supp. Figs. S4 and S5, including a comparison between the GLIC- and GluCl-derived models. Predicted modes of binding at the β3-β3 interface and in the α1 and β3 subunit helix bundles are shown in Supp. Figs. S6 and S7.

RESULTS

Photoreactive etomidate derivatives potentiate agonist binding to the purified α1β3 $GABA_AR$

The binding site(s) for anesthetics in the $GABA_AR$ are coupled energetically to the agonist site, as evidenced by the capacity of anesthetics of diverse structural classes to enhance GABA responses in cells and, for $GABA_AR$ in membrane fractions, to enhance agonist equilibrium binding affinity (31,32). This energetic coupling between sites is also preserved in the α1β3 $GABA_AR$ in membranes and after affinity purification (19), as evidenced by the etomidate enhancement of [^{3}H]muscimol binding. We found that *R*–azietomidate and TDBzl-etomidate (up to 100 μM) also enhanced [^{3}H]muscimol binding, by ~100 % and ~140 %, respectively (Figure 2). The concentrations for half-maximal potentiation by *R*-azietomidate and TDBzl-etomidate were ~3 μM and 0.8 μM, respectively. Both values are close to the general anesthetic potencies of these photoreactive anesthetics (EC_{50} = 2.2 μM & 0.7 μM, respectively (11,22)).

Characterization of the α1β3 $GABA_AR$

The purity of the α1β3 $GABA_AR$ was assessed by SDS-PAGE and Coomassie Blue stain, which revealed a major band of ~56 kDa, and minor bands of ~59, and ~61 kDa (Fig. 3A). When material from each of these bands was extracted and characterized by N-terminal protein sequencing, the primary sequence in both the 59 and 61 kDa bands was the N-terminus of the human $GABA_AR$ β3 subunit (variant 2, Fig. 3B), and the primary sequence in the 56 kDa band was the FLAG-tagged α1 subunit (Fig 3C). The β3 subunit was present in the α1 band at ~10 % the level of the α1 subunit, and, conversely, the α1 subunit was present in both β3 bands at 15 – 25 % the level of the β3 subunit.

The N-terminal sequence analyses also indicated that the β3 subunits in the 59 and 61 kDa bands differed in terms of their glycosylation at the first consensus N-linked glycosylation site in the subunit. The 11th cycle of Edman degradation of the β3 subunit and the 19th cycle of the FLAG-α1 subunit are predicted to contain asparagines which are potential sites of N-linked glycosylation. No PTH-Asn was released at those cycles of Edman degradation of the 56 kDa α1 subunit or the β3 subunit in the 61 kDa band, consistent with glycosylation at those positions. However, PTH-Asn was released in the 11th cycle for the β3 subunit in the 59 kDa band, which indicates that the β3 subunits in the 59 and 61 kDa bands are differentially glycosylated at that position.

Etomidate inhibits [^{3}H]azietomidate and [^{3}H]TDBzl-etomidate photolabeling of the α1β3 $GABA_AR$

$GABA_AR$ in elution buffer was photolabeled, and subunit photolabeling was determined by SDS-PAGE and liquid scintillation counting of excised gel bands (Fig. 4). In the presence of 1 mM GABA, [^{3}H]azietomidate (10 μM) photolabeled both the α1 and β3 subunits, and 100 μM etomidate inhibited by ~85 % the labeling of both subunits (Fig 4A). For the $GABA_AR$ photolabeled with 1 μM [^{3}H]TDBzl-etomidate, addition of GABA altered subunit photolabeling by < 10 % (not shown), and in the presence of GABA, etomidate (100 μM)

NIH-PA Author Manuscript

NIH-PA Author Manuscript

NIH-PA Author Manuscript

reduced [^{3}H]TDBzl-etomidate incorporation into the α1 subunit by 80 % and the β3 subunit by 60 % (Fig. 4B).

To determine the concentration dependence of [^{3}H]TDBzl-etomidate photolabeling, ^{3}H incorporation into the α1 and β3 subunits was determined by SDS-PAGE for $GABA_AR$ photolabeled by [^{3}H]TDBzl-etomidate at 0.5, 1.5 and 5 μM (total concentrations) in the absence and presence of 100 μM etomidate (Fig. 5). In the presence of etomidate, ^{3}H incorporation into each subunit increased linearly with [^{3}H]TDBzl-etomidate concentration, consistent with a non-specific (or low affinity) labeling component. The etomidate-inhibitable incorporation into each subunit was fit to a single-site binding model, with a [^{3}H]TDBzl-etomidate concentration of ~0.5 μM associated with half-maximal photolabeling. Based upon the calculated maximal etomidate-inhibitable photolabeling in the α1 subunit (2100 cpm or 0.12 pmol) and β3 subunit (1420 cpm or 0.08 pmol) and the amount of $GABA_AR$ receptor (20 pmol muscimol sites), ~0.6 % of α1 and 0.4 % of β3 subunits were photolabeled.

[^{3}H]Azietomidate photolabels α1Met-236 and β3Met-286 in the human α1β3 $GABA_AR$

To identify the photolabeled amino acids, $GABA_AR$ was photolabeled with [^{3}H]azietomidate (700 nM) on a preparative scale (130 pmol muscimol sites per condition) in the presence of 1 mM GABA and in the absence or presence of 100 μM etomidate, and samples containing primarily the α1 or β3 subunit were isolated by SDS-PAGE. The high degree of sequence conservation between bovine and human $GABA_AR$ subunits allowed us to use the previously developed proteolytic fragmentation and HPLC purification protocols (13) to identify the photolabeled amino acids in the $GABA_AR$ transmembrane domain. HPLC fractions enriched in a β3 subunit fragment beginning at the C-terminus of the β3 M2 helix and extending through M3 were isolated from EndoGlu-C digests (Supp. Fig. S8A), and fractions enriched in the α1 subunit fragment beginning at the N-terminus of αM1 were isolated from trypsin digests (Supp. Fig. S9A). Those HPLC fractions also contained other subunit fragments, but during sequence analysis the samples were treated with OPA at the cycles of Edman degradation containing a proline in βM3 (cycle 6, β3Pro-276) or in αM1 (cycle 11, α1Pro-233) to prevent further sequencing of contaminating fragments not containing Pro at those cycles (13,25).

During sequencing of the fragment beginning at β3Thr-271 with OPA treatment at cycle 6 (Figure 6A), the major peak of ^{3}H release was in cycle 16, establishing that β3Met-286 was labeled at 85 cpm/pmol and that the photolabeling was fully inhibited by etomidate. When HPLC fractions containing the fragment beginning at α1Ile-223 were sequenced (Figure 6B) with OPA treatment at cycle 11, the peak of ^{3}H release in cycle 14 established that [^{3}H]azietomidate also photolabeled α1Met-236 in αM1 (130 cpm/pmol) and that the photolabeling was also fully inhibitable by etomidate[2].

[^{3}H]TDBzl-etomidate photolabeling in $GABA_AR$ α1M1 and β3M3

The purified α1β3 $GABA_AR$ was photolabeled on a preparative scale with [^{3}H]TDBzl-etomidate at two concentrations (2 μM and 10 μM) in the presence of GABA and in the absence or presence of etomidate (100 μM), and gel band eluates enriched in β3 or α1 subunits were obtained by SDS-PAGE. Photolabeling of amino acids in β3M3 and α1M1 was characterized by sequencing appropriate rpHPLC fractions from EndoGlu-C digests of

[2]In the sequencing data of Figures 6A, 6B, and 7A, the peaks of ^{3}H release in cycle 3 and in cycle 7 (Fig. 6B) probably result from [^{3}H]azietomidate photolabeling of β3Met- 227 in βM1 (cycle 3) and α1Met-236 in αM1 (cycle 7). We have recently observed that Gln-Thr bonds are susceptible to cleavage under the acid conditions used to initiate sequencing (46). This amino acid pair is conserved in M1 of many $GABA_AR$ subunits, with a Thr 3 residues before β3Met-227 and 7 residues before α1Met-236. Direct demonstration of photolabeling of β3Met-227 by [^{3}H]azietomidate is shown in Figure 7.

NIH-PA Author Manuscript

NIH-PA Author Manuscript

NIH-PA Author Manuscript

the β3 subunits (Supp. Figs. S8 B & C) and EndoLys-C digests of α1 (Supp. Figs. S9 B & C). Representative sequencing data are presented in Fig. 6C-6F, and amino acid photolabeling efficiencies in the absence and presence of etomidate are summarized in Table 1 in comparison with data for [^{3}H]azietomidate.

For $GABA_AR$ photolabeled at 2 or 10 μM [^{3}H]TDBzl-etomidate, sequencing of the fractions containing the fragment beginning at β3Thr-271, with treatment with OPA in cycle 6, revealed a major peak of ^{3}H release in cycle 20 (Fig. 6C and 6E), which established that [^{3}H]TDBzl-etomidate photolabeled β3Val-290 and that etomidate inhibited that photolabeling by >90%. For the photolabeling at 10 μM [^{3}H]TDBzl-etomidate (Fig. 6E), there were also smaller peaks of ^{3}H release in cycles 16 and 18, which indicated photolabeling of β3Met-286 and βCys-288. While etomidate reduced photolabeling of β3Val-290 and βMet-286 by ≥ 90 % and ~60 %, respectively, photolabeling of βCys-288 was enhanced by ~10 % (Table 1).

[^{3}H]TDBzl-etomidate photolabeling of amino acids in αM1 was determined by sequencing rpHPLC fractions from EndoLys-C digests of α1 subunits that contained the fragment beginning at α1Ile-223 (Fig. 6D and 6F). During sequencing, samples were treated with OPA prior to cycle 11 (α1Pro-233) to prevent further sequencing of contaminating fragments. When material was sequenced from $GABA_AR$ photolabeled at 2 μM [^{3}H]TDBzl-etomidate (Fig. 6D), the peaks of ^{3}H release in cycles 12 and 14 identified photolabeling of α1Cys-234 and α1Met-236, respectively, with etomidate inhibiting photolabeling of those positions by 80 and 60 %. For the photolabeling at 10 μM [^{3}H]TDBzl-etomidate (Fig. 6F), the peak of ^{3}H release in cycle 14 indicated photolabeling of α1Met-236, which etomidate reduced by 30%, while photolabeling of α1Cys-234, if it occurred, was at <5% the efficiency of α1Met-236[3].

[^{3}H]Azietomidate and [^{3}H]TDBzl-etomidate also photolabel β3Met-227 in βM1

Sequence analysis of the rpHPLC fractions containing the major peak of ^{3}H from the EndoGlu-C digest of the [^{3}H]azietomidate photolabeled β3 subunit (Supp. Fig. S8A) identified a β3 subunit fragment beginning at β3Gly-203, 14 amino acids before the beginning of βM1 (Figure 7A). The major peak of ^{3}H release in cycle 25 was consistent with photolabeling of β3Met-227, with etomidate inhibiting that photolabeling by > 95 %[2].

Cleavage of the bond between β3Thr-202 and β3Gly-203 was unlikely to be produced by EndoGlu-C, which has specificity for cleavage C-terminal to acidic amino acid side chains. However, [^{3}H]azietomidate photolabeling of β3Met-227 was confirmed by sequence analysis of HPLC fractions from EndoGlu-C digests of [^{3}H]azietomidate photolabeled β subunits from an independent photolabeling experiment (Fig. 7B). In this case, a fragment was sequenced beginning at β3His-191, an expected EndoGlu-C cleavage site, and the sample was treated with OPA at cycle 16 (β3Pro-206). The peak of ^{3}H release in cycle 37 confirmed labeling at β3Met-227 in the presence (or absence) of GABA. [^{3}H]TDBzl-etomidate at 10 μM also photolabeled β3Met-227, but at only ~20 % the efficiency of α1Met-236 (Table 1, data not shown). Thus, β3Met-227 was photolabeled by [^{3}H]azietomidate and [^{3}H]TDBzl-etomidate with the same pharmacological specificity as α1Met-236 in αM1 (Table 1).

[3]The peaks of ^{3}H release in cycles 7 and 9 (Figure 6F) originate from photolabeling in βM3 which contaminates this α1 subunit sample.

NIH-PA Author Manuscript

NIH-PA Author Manuscript

NIH-PA Author Manuscript

Does [^{3}H]TDBzl-etomidate photolabel amino acids in other transmembrane helices?

Since TDBzl-etomidate can react with aliphatic as well as nucleophilic amino acid side chains, we also sequenced appropriate HPLC fractions to determine whether it photolabeled amino acids in α1M2, which can be isolated from α1 subunit EndoGlu-C digests, or in α1M4, isolated from EndoLys-C digests. From $GABA_AR$s photolabeled with [^{3}H]TDBzl-etomidate, sequence analyses of fragments beginning at α1Ser-251 (2 pmol) before α1M2 and of α1Thr-377 (10 pmol) before α1M4 established that any photolabeling of amino acids within α1M2 or α1M4 was at < 5 cpm/pmol, i.e. at less than 5 % the photolabeling of α1Met-236 (data not shown).

To evaluate photolabeling in β3M2, an aliquot of intact β3 subunit, isolated from the α1β3 $GABA_AR$ photolabeled with 2 μM [^{3}H]TDBzl-etomidate, was digested chemically with BNPS-skatol and sequenced. BNPS-skatol cleaves after Trp residues, of which there are only 7 in the β3 subunit. Cleavage at β3Trp-241 near the C-terminus of βM1 allowed sequencing through β3M2 (12 pmol initial yield (Supplementary Figure S10)). No releases of ^{3}H were detected above background, which indicates that any photolabeling of amino acids in β3M2, if it occurred, was at < 5 cpm/pmol. i.e. at less than 10% the photolabeling of β3Val-290.

DISCUSSION

In this report we identified the amino acids photolabeled in a purified, expressed human FLAG-α1β3 $GABA_AR$ by two photoreactive etomidate analogs, [^{3}H]TDBzl-etomidate, which possesses broad amino acid side chain reactivity, and [^{3}H]azietomidate, which can react with nucleophilic but not aliphatic amino acid side chains and was used previously to identify two residues, αMet-236 and βMet-286, photolabeled in a heterogeneous population of $GABA_AR$ purified from bovine brain (13). We interpret the photolabeling results by use of α1β3 $GABA_AR$ homology models based upon the recently solved crystal structures of two detergent-solubilized, homopentameric ligand-gated ion channels, GLIC, a proton-gated cation-selective channel (PDB:3P50) (20), and GluCl, a glutamate-gated chloride channel (PDB code 3RHW) (21). GLIC and GluCl each have a higher degree of amino acid sequence conservation with the $GABA_AR$ subunit M3 and M4 helices than do the nAChR subunits, and this results in a more confident alignment of those $GABA_AR$ regions in these homology models than in models based upon the structure of the *Torpedo* nAChR (PDB code 2BG9) (14). As described in Methods, the locations of the photolabeled $GABA_AR$ amino acids are essentially equivalent in the homology models based upon these two structures, but differ subtly from those in the model we developed previously (13) based upon the *Torpedo* nAChR structure[4].

Table 1 summarizes for comparison purposes, the efficiencies of [^{3}H]TDBzl-etomidate and [^{3}H]azietomidate photoincorporation into the $GABA_AR$ amino acids. The locations of the photolabeled amino acids in a $GABA_AR$ homology model based upon the structure of GLIC are shown in Fig. 8 in views of the $GABA_AR$ transmembrane domain from the base of the extracellular domain (Figs. 8B & D) and from the lipid towards the β3-α1 interface (Figs. 8C, E and F). The photolabeled amino acids β3Met-286, β3Val-290, and α1Met-236 each project into the interface between the β3 and α1 subunits. The photolabeled Cys in βM3 (β3Cys-288) and αM1 (α1Cys-234) are not accessible from the pocket at the β3-α1 interface, despite their proximity in primary structure to β3Met-286/β3Val-290 or α1Met-236. Rather, they project into the β3 and α1 helix bundle pockets, respectively. In a β3α1β3α1β3

[4]Comparisons of the locations of the photolabeled amino acids in the GLIC-, GluCl-, and nAChR- derived homology models are shown in Supplemental Figures S2 & S3.

NIH-PA Author Manuscript

NIH-PA Author Manuscript

NIH-PA Author Manuscript

$GABA_AR$ the photolabeled β3Met-227 in βM1 is located at the interface between adjacent β3 subunits in proximity to the photolabeled amino acids in βM3 of the adjacent subunit (Figs. 8B and C). In addition to the identification of photolabeled amino acids in αM1, βM1, and βM3, we also established that any [^{3}H]TDBzl-etomidate photolabeling of amino acids in in β3M2, α1M2, or α1M4, if it occurred, was at <5 % the efficiency of the incorporation in α1Met-236 in α1M1.

Photolabeling and docking studies define a restricted etomidate binding site at the β3-α1 subunit interface

TDBzl-etomidate, in stick representation, is included in Figs. 8D - 8F docked in a pocket at the β3-α1 interface in its energy-minimized orientation in proximity to amino acids from β3M3, β3M2, α1M1 and α1M2, including β3Asn-265 in M2, an etomidate and propofol sensitivity determinant *in vitro* and *in vivo* (9,10), and αLeu-232, a position in αM1 identified as a sensitivity determinant for volatile anesthetics (1,33). This location is similar to the position in the GluCl structure of ivermectin (21), a molecule much larger than TDBzl-etomidate, which occupies this intersubunit binding site extending between the M3 and M1 helices from the lipid interface to the M2 helices.

In a series of docking calculations testing the effects of different diameter binding site spheres and different initial sets of TDBzl-etomidate conformations and orientations (see Methods), in each case for >90 of the 100 lowest energy docking solutions, *R*-TDBzl-etomidate was oriented with its diazirine carbon within 5 Å of the photolabeled residues β3Met-286, β3Val-290, and α1Met-236, and to α1Leu-232. The etomidate benzyl group was oriented toward β3Asn-265/β3Arg-269 (positions M2-15 and M2-19 in βM2) and α1Gln-229 in αM1/α1Leu-269 (position M2-14 in αM2) (Supp. Fig. S4). TDBzl-etomidate is also predicted to be in proximity to β3Phe-289 and α1Pro-233 (Fig. 8F), which are determinants of the shape of this pocket and, therefore, are predicted to be important determinants of the energetics of binding of TDBzl-etomidate. TDBzl-etomidate was also predicted to bind in a similar orientation in this pocket in a $GABA_AR$ homology model based upon the structure of GluCl (Supp. Fig. S5).

Since TDBzl-etomidate can react broadly with most amino acid side chains, its photolabeling of β3Val-290, β3Met-286, and α1Met-236, in conjunction with the absence of photolabeling of amino acids in α1M2 and β3M2 and the results of the computational docking studies, provide strong evidence defining the orientation of TDBzl-etomidate in this binding site. Etomidate inhibits photolabeling by 2 μM [^{3}H]TDBzl-etomidate of β3Val-290 by ~90 % and photolabeling of β3Met-286 and α1Met-236 by ~60 % (Table 1). Although it is not clear why etomidate inhibits [^{3}H]TDBzl-etomidate photolabeling of β3Val-290 more completely, the fact that etomidate inhibits [^{3}H]azietomidate photolabeling of β3Met-286 and α1Met-236 by >90% establishes that etomidate, TDBzl-etomidate, and azietomidate all bind to this site. *R*-Etomidate (molecular volume 205 Å^3) or *R*-azietomidate (volume, 240 Å^3) are also predicted to bind within this pocket. However, their predicted orientations within the pocket are less constrained than that of *R*-TDBzl-etomidate (volume, 285 Å^3), as a consequence of their smaller sizes.

Photolabeling of β3Met-227 in βM1

[^{3}H]Azietomidate and [^{3}H]TDBzl-etomidate also photolabel β3Met-227, a position in βM1 equivalent to α1Leu-232. [^{3}H]Azietomidate photolabeled β3Met-227 at an efficiency similar to that of α1Met-236 or β3Met-286 (Table 1), and etomidate inhibited [^{3}H]azietomidate photolabeling of β3Met-227 by > 95 %. In the β3α1β3α1β3 $GABA_AR$ homology model, β3Met-227 is positioned at a β3-β3 interface and also at the α1-β3 interface. Docking calculations predict that TDBzl-etomidate can bind in the pocket at the β3-β3 interface,

NIH-PA Author Manuscript

NIH-PA Author Manuscript

NIH-PA Author Manuscript

although its orientation may be less constrained than at the β3-α1 interface (Supp. Fig. S6). Interestingly, β3Met-227 was not equivalently photolabeled in the βαβαγ $GABA_AR$s purified from bovine brain (13), which lack a β-β interface. The presence or absence of etomidate-inhibitable photolabeling of β3Met-227 in an expressed β3α1β3α1γ2 $GABA_AR$ will reveal whether etomidate is binding at the unnatural β3-β3 interface in the αβ $GABA_AR$.

Photolabeling of β3Cys-288 in βM3 and α1Cys-234 in αM1

[^{3}H]TDBzl-etomidate also photolabels β3Cys-288 and α1Cys-234, which in the homology model are located within the pockets in the β3 and α1 subunit helix bundles, respectively (Supp. Fig. S7). $GABA_AR$ β3Cys-288 and α1Cys-234 are equivalent to GLIC Ile-262 and Met-205, respectively, which in the homopentameric GLIC crystal structure are adjacent in the subunit helix bundle and within 5 Å of the bound propofol (20).

The photolabeling of β3Cys-288 appears consistent with background, non-specific photolabeling, since aromatic diazirines such as [^{3}H]TDBzl-etomidate are more reactive with Cys than with other amino acid side chains and the observed photolabeling increases from 2 μM to 10 μM, but is not inhibited by etomidate (Table 1). However, in the $GABA_AR$ homology model β3Cys-288 is not exposed on the receptor surface, but is located deep within the β3 subunit helix bundle pocket. This suggests that TDBzl-etomidate, but not etomidate, can bind with low affinity within this pocket.

α1Cys-234 is located within the α1 subunit helix bundle pocket, and its unusual pharmacology of photolabeling suggests the [^{3}H]TDBzl-etomidate can bind with low affinity within that pocket only when the etomidate/TDBzl-etomidate binding site at the interface between β3 and α1 subunits is unoccupied. [^{3}H]TDBzl-etomidate at 2 μM photolabeled α1Cys-234 at ~50 % the efficiency of α1Met-236, and etomidate inhibited that photolabeling (Fig. 6D and Table 1). However, at 10 μM [^{3}H]TDBzl-etomidate, photolabeling of α1Cys-234 was greatly reduced relative to α1Met-236 and insensitive to etomidate (Fig. 6F and Table 1). Since [^{3}H]TDBzl-etomidate at ~1 μM produced ~50 % of maximal etomidate-inhibitable $GABA_AR$ photolabeling (Fig. 5), these results suggest that α1Cys-234 is not accessible to [^{3}H]TDBzl-etomidate when either etomidate or [^{3}H]TDBzl-etomidate occupies the site at that β3-α1 interface. α1Cys-234 is accessible to [^{3}H]TDBzl-etomidate when that interfacial site is unoccupied, though TDBzl-etomidate or etomidate may occupy the site at the other β3-α1 interface.

Diversity of anesthetic binding sites in pentameric ligand-gated ion channels

Given the structural diversity of general anesthetics that act as positive $GABA_AR$ modulators at clinically relevant concentrations, including small volatiles such as isoflurane and desflurane as well as etomidate, barbiturates and neurosteroids, it is unlikely that all anesthetics bind to a common class of sites; i.e. at a subunit interface or within a subunit transmembrane helix bundle. Within crystals of GLIC equilibrated with pure propofol or desflurane, which in functional studies act as inhibitors of channel gating, the two anesthetics are bound to intrasubunit sites at slightly different depths within the transmembrane helix bundle (20). In the *Torpedo* nAChR, photoaffinity labeling studies establish that small drugs (vol. <240 Å^3) that act as allosteric inhibitors, including benzophenone, 3-(trifluoromethyl)-3-(*m*-iodophenyl)diazirine), and the general anesthetics halothane and azietomidate, also bind in a state-dependent manner to an intrasubunit site formed by the δ subunit transmembrane helix bundle (34-38). However, TDBzl-etomidate, which is larger in size (vol. = 285 Å^3) and acts as a nAChR potentiator while binding only weakly in the ion channel, binds to a site at the interface between γ and α subunits (23).

NIH-PA Author Manuscript

NIH-PA Author Manuscript

NIH-PA Author Manuscript

Thus, it remains to be determined whether a drug can act as a $GABA_AR$ potentiator when it binds to an intrasubunit site.

General anesthetic binding sites in $GABA_ARs$

Propofol has been predicted to bind in proximity to βMet-286, since propofol reduced the kinetics of modification of a cysteine substituted at that position (39). However, propofol does not bind in a mutually exclusive manner with etomidate, since propofol acts as an allosteric inhibitor of [^{3}H]azietomidate photolabeling of βMet-286 and αMet-236 (40).

The etomidate binding site at the β-α interface identified by [^{3}H]azietomidate and [^{3}H]TDBzl-etomidate cannot be a neurosteroid binding site, since neurosteroids enhance, rather than inhibit, $GABA_AR$ photolabeling by [^{3}H]azietomidate (41). In addition, the single amino acid substitutions in βM3 and αM1 identified as neurosteroid activation determinants (18) are not located at the β-α interface and do not contribute to a common binding site (7,41).

Volatile anesthetics were proposed to bind to intrasubunit pockets formed by the transmembrane bundle of helices, based upon the locations in an early $GABA_AR$ structural model of anesthetic sensitivity determinants in αM1 (αLeu-232), αM2 (αM2-15), and αM3 (α2Ala-291, equivalent to β3Met-286 (1,33). However, in $GABA_AR$ structural models based upon the structures of the nAChR, GLIC, or GluCl, αLeu-232 and αAla291 are each positioned at interfaces with the β subunit rather than within the helix bundle (Fig. 8 and Supp. Figs. S2-S5, see also (42)). Further studies using photoreactive analogs of propofol (43), neurosteroids (44), or volatile anesthetics (45) will be necessary to determine whether any of these drugs binds in proximity to the etomidate binding site at the β-α interface, or, alternatively, to intrasubunit sites within a subunit transmembrane helix bundle or at the protein-lipid interface.

Supplementary Material

Refer to Web version on PubMed Central for supplementary material.

Acknowledgments

We thank Dr. Ayman Hamouda for many helpful comments concerning this manuscript.

Abbreviations

OPA	*o*-phthalaldehyde
GABA	γ-aminobutyric acid
$GABA_AR$	γ-aminobutyric acid type-A receptor
nAChR	nicotinic acetylcholine receptor
azietomidate	2-(3-methyl-3H-diaziren-3-yl) ethyl 1-(1-phenylethyl)-1H-imidazole-5-carboxylate
TDBzl-etomidate	4-[3-(trifluoromethyl)-3*H*-diazirin-3-yl]benzyl 1-(1-phenylethyl)-1*H*-imidazole-5-carboxylate
CHAPS	3-[(3-cholamidopropyl)dimethylammonio]-1-propanesulfonate
EndoLys-C	*Lysobacter enzymogenes* Endoproteinase Lys-C
EndoGlu-C	*S. aureus* Glutamic-C endopeptidase

NIH-PA Author Manuscript

NIH-PA Author Manuscript

NIH-PA Author Manuscript

rpHPLC	revered phase high performance liquid chromatography
BNPS-skatol	3-bromo-3-methyl-2-(2-nitrophenylthio)-3H-indole

REFERENCES

1. Hemmings HC, Akabas MH, Goldstein PA, Trudell JR, Orser BA, Harrison NL. Emerging molecular mechanisms of general anesthetic action. Trends Pharmacol. Sci. 2005; 26:503–510. [PubMed: 16126282]
2. Franks NP. General anaesthesia: from molecular targets to neuronal pathways of sleep and arousal. Nature Rev. Nsci. 2008; 9:370–386.
3. Forman SA. Clinical and molecular pharmacology of etomidate. Anesthesiology. 2011; 114:695–707. [PubMed: 21263301]
4. Tomlin SL, Jenkins A, Lieb WR, Franks NP. Stereoselective effects of etomidate optical isomers on gamma-aminobutyric acid type A receptors and animals. Anesthesiology. 1998; 88:708–717. [PubMed: 9523815]
5. Rusch D, Zhong HJ, Forman SA. Gating allosterism at a single class of etomidate sites on alpha(1)beta(2)gamma(2L) GABA(A) receptors accounts for both direct activation and agonist modulation. J. Biol. Chem. 2004; 279:20982–20992. [PubMed: 15016806]
6. Cederholm JME, Schofield PR, Lewis TM. Gating mechanisms in Cys-loop receptors. Eur. Biophys. J. 2009; 39:37–49. [PubMed: 19404635]
7. Miller PS, Smart TG. Binding, activation and modulation of Cys-loop receptors. Trends Pharmacol. Sci. 2010; 31:161–174. [PubMed: 20096941]
8. Hill-Venning C, Belelli D, Peters JA, Lambert JJ. Subunit-dependent interaction of the general anaesthetic etomidate with the γ-aminobutyric acid type A receptor. Br. J. Pharmacol. 1997; 120:749–756. [PubMed: 9138677]
9. Belelli D, Lambert JJ, Peters JA, Wafford K, Whiting PJ. The interaction of the general anesthetic etomidate with the gamma-aminobutyric acid type A receptor is influenced by a single amino acid. Proc. Nat. Acad. Sci. USA. 1997; 94:11031–11036. [PubMed: 9380754]
10. Jurd R, Arras M, Lambert S, Drexler B, Siegwart R, Crestani F, Zaugg M, Vogt KE, Ledermann B, Antkowiak B, Rudolph U. General anesthetic actions in vivo strongly attenuated by a point mutation in the GABA(A) receptor beta 3 subunit. FASEB J. 2003; 17:250–252. [PubMed: 12475885]
11. Husain SS, Ziebell MR, Ruesch D, Hong F, Arevalo E, Kosterlitz JA, Olsen RW, Forman SA, Cohen JB, Miller KW. 2-(3-methyl-3H-diaziren-3-yl) ethyl 1-(1-phenylethyl)-1H-imidazole-5-carboxylate: A derivative of the stereoselective general anesthetic etomidate for photolabeling ligand-gated ion channels. J. Med. Chem. 2003; 46:1257–1265. [PubMed: 12646036]
12. Liao M, Sonner JM, Husain SS, Miller KW, Jurd R, Rudolph U, Eger EI. *R*(+)etomidate and the photoactivable *R*(+)azietomidate have comparable anesthetic activity in wild-type mice and comparably decreased activity in mice with a N265M point mutation in the gamma-aminobutyric acid receptor β3 subunit. Anesth. Analg. 2005; 101:131–135. [PubMed: 15976219]
13. Li G-D, Chiara DC, Sawyer GW, Husain SS, Olsen RW, Cohen JB. Identification of a GABAA receptor anesthetic binding site at subunit interfaces by photolabeling with an etomidate analog. J. Neurosci. 2006; 26:11599–11605. [PubMed: 17093081]
14. Unwin N. Refined structure of the nicotinic acetylcholine receptor at 4 Å resolution. J. Mol. Biol. 2005; 346:967–989. [PubMed: 15701510]
15. Ziebell MR, Nirthanan S, Husain SS, Miller KW, Cohen JB. Identification of binding sites in the nicotinic acetylcholine receptor for [^{3}H]azietomidate, a photoactivatable general anesthetic. J. Biol. Chem. 2004; 279:17640–17649. [PubMed: 14761946]
16. Das J. Aliphatic diazirines as photoaffinity probes for proteins: Recent developments. Chem. Revs. 2011; 111:4405–4417. [PubMed: 21466226]

NIH-PA Author Manuscript

NIH-PA Author Manuscript

NIH-PA Author Manuscript

17. Ernst M, Bruckner S, Boresch S, Sieghart W. Comparative models of GABA(A) receptor extracellular and transmembrane domains: Important insights in pharmacology and function. Mol. Pharmacol. 2005; 68:1291–1300. [PubMed: 16103045]
18. Hosie AM, Wilkins ME, Da Silva HMA, Smart TG. Endogenous neurosteroids regulate $GABA_A$ receptors through two discrete transmembrane sites. Nature. 2006; 444:486–489. [PubMed: 17108970]
19. Dostalova Z, Liu AP, Zhou XJ, Farmer SL, Krenzel ES, Arevalo E, Desai R, Feinberg-Zadek PL, Davies PA, Yamodo IH, Forman SA, Miller KW. High-level expression and purification of Cys-loop ligand-gated ion channels in a tetracycline-inducible stable mammalian cell line: GABA(A) and serotonin receptors. Prot. Sci. 2010; 19:1728–1738.
20. Nury H, Van Renterghem C, Weng Y, Tran A, Baaden M, Dufresne V, Changeux JP, Sonner JM, Delarue M, Corringer PJ. X-ray structures of general anaesthetics bound to a pentameric ligand-gated ion channel. Nature. 2011; 469:428–431. [PubMed: 21248852]
21. Hibbs RE, Gouaux E. Principles of activation and permeation in an anion-selective Cys-loop receptor. Nature. 2011; 474:54–60. [PubMed: 21572436]
22. Husain SS, Nirthanan S, Ruesch D, Solt K, Cheng Q, Li GD, Arevalo E, Olsen RW, Raines DE, Forman SA, Cohen JB, Miller KW. Synthesis of trifluoromethylaryl diazirine and benzophenone derivatives of etomidate that are potent general anesthetics and effective photolabels for probing sites on ligand-gated ion channels. J. Med. Chem. 2006; 49:4818–4825. [PubMed: 16884293]
23. Nirthanan S, Garcia G, Chiara DC, Husain SS, Cohen JB. Identification of binding sites in the nicotinic acetylcholine receptor for TDBzl-etomidate, a photoreactive positive allosteric effector. J.Biol.Chem. 2008; 283:22051–22062. [PubMed: 18524766]
24. Crimmins DL, McCourt DW, Thoma RS, Scott MG, Macke K, Schwartz BD. *In situ* chemical cleavage of proteins immobilized to glass-fiber and polyvinylidenedifluoride membranes: Cleavage at tryptophan residues with 2-(2'¦-nitrophenylsulfenyl)-3-methyl-3'¦-bromoindolenine to obtain internal amino acid sequence. Anal. Biochem. 1990; 187:27–38. [PubMed: 2372117]
25. Brauer AW, Oman CL, Margolies MN. Use of *o*-phthalaldehyde to reduce background during automated Edman degradation. Anal. Biochem. 1984; 137:134–142. [PubMed: 6428262]
26. Middleton RE, Cohen JB. Mapping of the acetylcholine binding site of the nicotinic acetylcholine receptor: [^{3}H]-nicotine as an agonist photoaffinity label. Biochemistry. 1991; 30:6987–6997. [PubMed: 2069955]
27. Tretter V, Ehya N, Fuchs K, Sieghart W. Stoichiometry and assembly of a recombinant GABA(A) receptor subtype. J. Neurosci. 1997; 17:2728–2737. [PubMed: 9092594]
28. Baumann SW, Baur R, Sigel E. Subunit arrangement of γ-aminobutyric acid type A receptors. J.Biol.Chem. 2001; 276:36275–36280. [PubMed: 11466317]
29. Bali M, Jansen M, Akabas MH. GABA-induced intersubunit conformational movement in the $GABA_A$ receptor α1M1−β2M3 transmembrane subunit interface: Experimental basis for homology modeling of an intravenous anesthetic binding site. J.Neurosci. 2009; 29:3083–3092. [PubMed: 19279245]
30. Wu G, Robertson DH, Brooks CLI, Vieth M. Detailed analysis of grid-based molecular docking: A case study of CDOCKER--A CHARMm-based MD docking algorithm. J. Comp. Chem. 2003; 24:1549–1562. [PubMed: 12925999]
31. Sieghart W. Structure and pharmacology of gamma-aminobutyric acid A receptor subtypes. Pharmacol. Rev. 1995; 47:181–234. [PubMed: 7568326]
32. Carlson, BX.; Hales, TG.; Olsen, RW. $GABA_A$ Receptors and Anesthesia.. In: Yaksh, TL., editor. Anesthesia: Biologic Foundations. Lippincott-Raven Publishers; Philadelphia: 1997. p. 259-275.e. al.
33. Jenkins A, Greenblatt EP, Faulkner HJ, Bertaccini E, Light A, Lin A, Andreasen A, Viner A, Trudell JR, Harrison NL. Evidence for a common binding cavity for three general anesthetics within the GABA(A) receptor. J. Neurosci. 2001; 21:U7–U10.
34. Chiara DC, Dangott LJ, Eckenhoff RG, Cohen JB. Identification of nicotinic acetylcholine receptor amino acids photolabeled by the volatile anesthetic halothane. Biochemistry. 2003; 42:13457–13467. [PubMed: 14621991]

NIH-PA Author Manuscript

NIH-PA Author Manuscript

NIH-PA Author Manuscript

35. Garcia G, Chiara DC, Nirthanan S, Hamouda AK, Stewart DS, Cohen JB. [^{3}H]Benzophenone photolabeling identifies state-dependent changesin nicotinic acetylcholine receptor structure. Biochemistry. 2007; 46:10296–10307. [PubMed: 17685589]
36. Chiara DC, Hong FH, Arevalo E, Husain SS, Miller KW, Forman SA, Cohen JB. Time-resolved photolabeling of the nicotinic acetylcholine receptor by [^{3}H]Azietomidate, an open-state inhibitor. Mol. Pharmacol. 2009; 75:1084–1095. [PubMed: 19218367]
37. Yamodo IH, Chiara DC, Cohen JB, Miller KW. Conformational changes in the nicotinic acetylcholine receptor during gating and desensitization. Biochemistry. 2010; 49:156–165. [PubMed: 19961216]
38. Hamouda AK, Stewart DS, Husain SS, Cohen JB. Multiple transmembrane binding sites for p-trifluoromethyldiazirinyl-etomidate, a photoreactive *Torpedo* nicotinic acetylcholine receptor allosteric inhibitor. J. Biol. Chem. 2011; 286:20466–20477. [PubMed: 21498509]
39. Bali M, Akabas MH. Defining the propofol binding site location on the $GABA_A$ receptor. Mol. Pharmacol. 2004; 65:68–76. [PubMed: 14722238]
40. Li GD, Chiara DC, Cohen JB, Olsen RW. Numerous classes of general anesthetics inhibit etomidate binding to γ-aminobutyric acid type A ($GABA_A$) receptors. J. Biol. Chem. 2010; 285:8615–8620. [PubMed: 20083606]
41. Li G-D, Chiara DC, Cohen JB, Olsen RW. Neurosteroids allosterically modulate binding of the anesthetic etomidate to γ-aminobutyric acid type A receptors. J. Biol. Chem. 2009; 284:11771–11775. [PubMed: 19282280]
42. Bertaccini EJ, Wallner B, Trudell JR, Lindahl E. Modeling anesthetic binding sites within the glycine alpha one receptor based on prokaryotic ion channel templates: The Problem with TM4. J. Chem. Inform. Model. 2010; 50:2248–2255.
43. Hall MA, Xi J, Lor C, Dai S, Pearce R, Dailey WP, Eckenhoff RG. *m*-Azipropofol (AziPm) a photoactive analogue of the intravenous general anesthetic propofol. J. Med. Chem. 2010; 53:5667–5675. [PubMed: 20597506]
44. Darbandi-Tonkabon R, Hastings WR, Zeng C-M, Akk G, Manion BD, Bracamontes JR, Steinbach JH, Mennerick S, Covey DF, Evers AS. Photoaffinity labeling with a neuroactive steroid analogue. J. Biol. Chem. 2003; 278:13196–13206. [PubMed: 12560326]
45. Eckenhoff RG, Xi J, Shimaoka M, Bhattacharji A, Covarrubias M, Dailey WP. Azi-isoflurane, a photolabel analog of the commonly used inhaled general anesthetic isoflurane. ACS Chem. Nsci. 2010; 1:139–145.
46. Chiara DC, Hamouda AK, Ziebell MR, Mejia LA, Garcia G, Cohen JB. [^{3}H]Chlorpromazine photolabeling of the *Torpedo* nicotinic acetylcholine receptor identifies two state-dependent binding sites in the ion channel. Biochemistry. 2009; 48:10066–10077. [PubMed: 19754159]

NIH-PA Author Manuscript

NIH-PA Author Manuscript

NIH-PA Author Manuscript

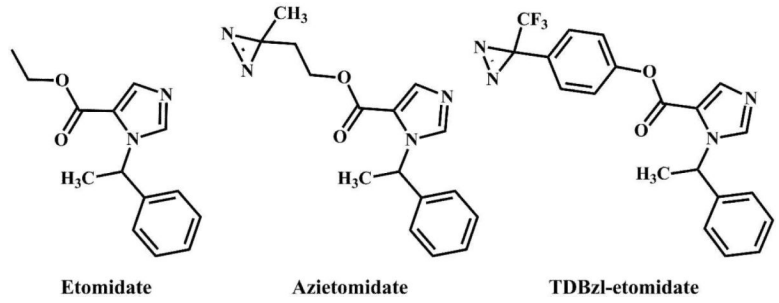

FIGURE 1.
Structures of etomidate and its photoreactive derivatives.

NIH-PA Author Manuscript

NIH-PA Author Manuscript

NIH-PA Author Manuscript

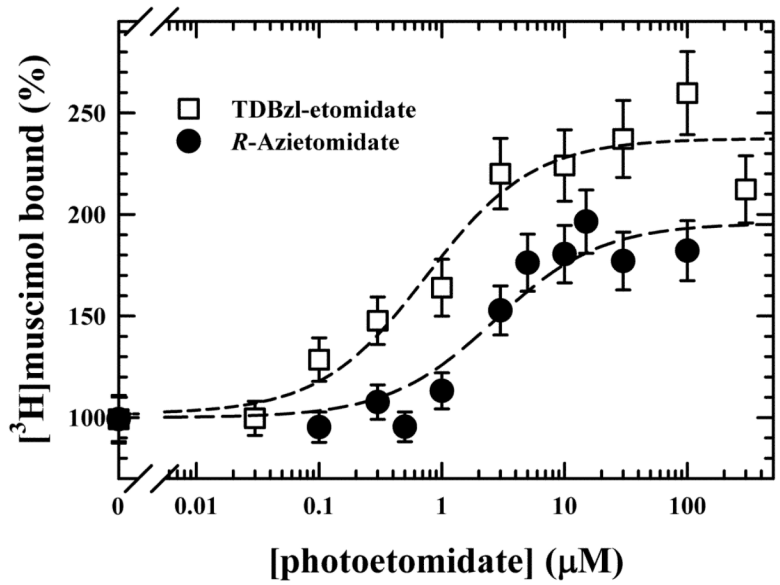

FIGURE 2. Modulation of [^{3}H]muscimol binding to purified α1β3 GABA$_A$R by photoreactive etomidate derivatives

Purified α1β3 GABA$_A$R was incubated for 1 h in binding buffer containing 5 mM CHAPS with 1 nM [^{3}H]muscimol, a concentration sufficient to occupy ~10% of binding sites, and various concentrations of TDBzl–etomidate ([box3]) or *R*–azietomidate (●), and then binding was determined by filtration, as described in Methods. Each data point was determined in triplicate and plotted as mean ± SD. In this typical experiment, the cpm for the total binding was 4890 ± 21 in the absence of anesthetic, and the nonspecific binding (+ 1 mM GABA) was 400 ± 56 cpm. For R-azietomidate and TDBzl-etomidate, the concentrations producing half maximal potentiation were 2.7 ± 1.0 μM and 0.8 ± 0.3 μM, respectively, with maximal potentiations of 200 ± 10% and 240 ± 10%.

NIH-PA Author Manuscript

NIH-PA Author Manuscript

NIH-PA Author Manuscript

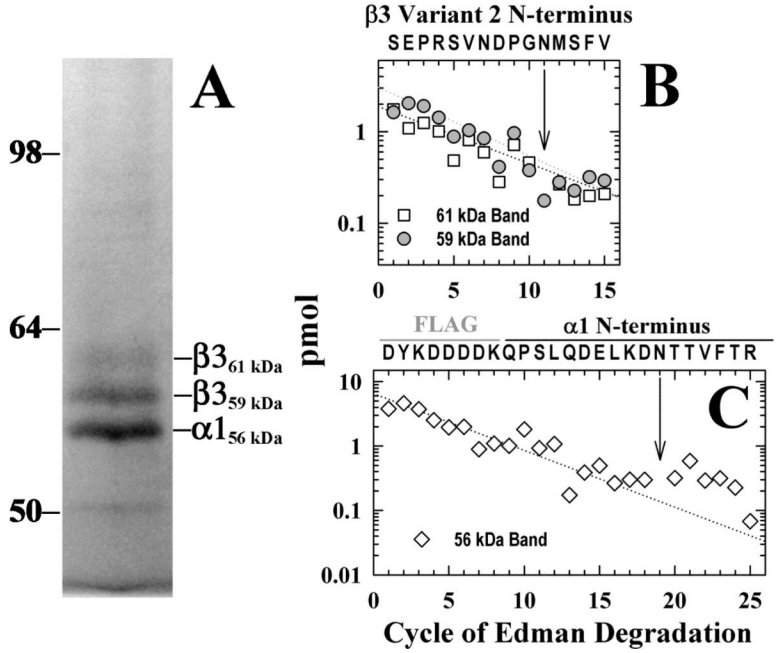

FIGURE 3. SDS-PAGE and N-terminal sequence analyses of purified α1β3 $GABA_AR$

A, The purity of a $GABA_AR$ preparation was assessed by SDS-PAGE (9 pmol muscimol binding sites, Coomassie blue stain). **B** and **C**, pmol of PTH-amino acids detected during sequencing of material eluted from gel bands of 59 and 61 kDa (**B**) and 56 kDa (**C**). The N-terminus of the human $GABA_AR$ β3 subunit (variant 2) was the primary sequence detected in the 59 and 61 kDa bands (I_0 = 3.0 and 1.9 pmol, respectively), and the FLAG-tagged N-terminus of the α1 subunit was the primary sequence in the 56 kDa band (I_0 = 6.5 pmol). The 56 kDa band contained as the secondary sequence 0.6 pmol of β3, and the 59 kDa and 61 kDa bands each contained 0.4 pmol of FLAG-α1. The β3 subunits in the 59 and 61 kDa bands are differentially glycosylated, as evidenced by the level of PTH-Asn detected in Edman degradation cycle 11 (arrow, see Results).

NIH-PA Author Manuscript

NIH-PA Author Manuscript

NIH-PA Author Manuscript

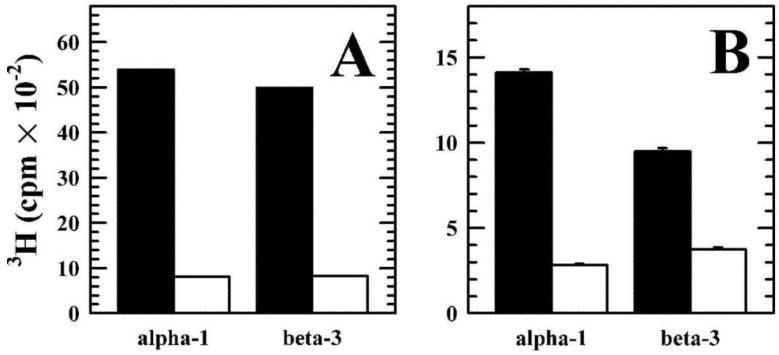

FIGURE 4. Etomidate-inhibitable [^{3}H]azietomidate and [^{3}H]TDBzl-etomidate photoincorporation into α1β3 GABA$_A$R subunits

^{3}H incorporation was determined by liquid scintillation counting for the gel bands enriched in α1 or β3 subunits isolated by SDS-PAGE from α1β3 GABA$_A$R photolabeled in the presence of 1 mM GABA with 10 μM [^{3}H]azietomidate (**A**, 16 pmol muscimol sites) or 1 μM [^{3}H]TDBzl-etomidate (**B**, 3 pmol muscimol sites) in the absence (black) or presence (white) of 100 μM etomidate. For the β3 subunits, the combined ^{3}H cpm in the 59 and 61 kDa gel bands are plotted.

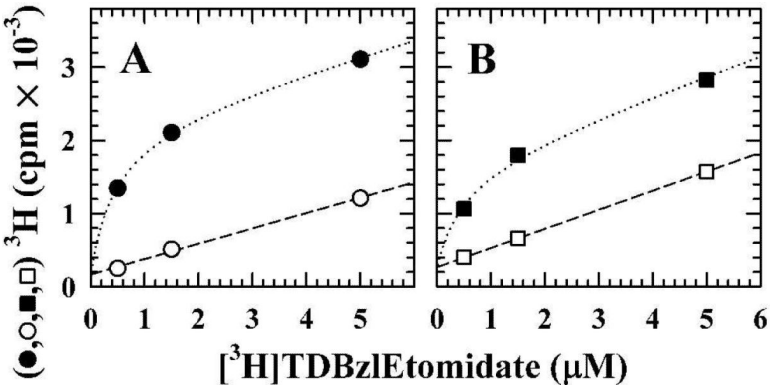

FIGURE 5. Concentration dependence of [^{3}H]TDBzl-etomidate photolabeling of α1β3 GABA$_A$R

^{3}H incorporation into gel bands enriched in α1 (**A**) or β3 (**B**) subunits isolated by SDS-PAGE from α1β3 GABA$_A$R (20 pmol muscimol sites) photolabeled by [^{3}H]TDBzl-etomidate in the presence of 1 mM GABA and in the absence (●,■) or presence (○,□) of 100 μM etomidate. For the samples photolabeled in the presence of etomidate, the subunit cpm increased linearly with [^{3}H]TDBzl-etomidate concentration, with slope B_{ns} and intercept, *b*. For the samples photolabeled in the absence of etomidate, the dotted lines are the fits of the subunit cpm to the equation $f(x) = [B_{max}/(1+K/x)]+B_{ns}\times x + b$, where $f(x)$ is the cpm at concentration *x*, *K* is the apparent dissociation constant in μM, and B_{max} the maximal etomidate-inhibitable ^{3}H incorporation (in cpm). Values for B_{ns} and *b* were determined from the subunit photolabeling in the presence of 100 μM etomidate. **A**, For the α1 subunit, K = 0.45 ± 0.04 μM and B_{max} = 2,080 ± 50 cpm (120 fmol ^{3}H) (*Bns* = 210 ± 10 cpm/ M, and *b* = 170 ± 30 cpm); **B**, for the β3 subunit, K = 0.50 ± 0.18 μM and B_{max} = 1,420 ± 130 cpm (80 fmol ^{3}H) (B*ns* = 260 ± 10 cpm/μM, and *b* = 270 ± 10 cpm).

NIH-PA Author Manuscript NIH-PA Author Manuscript NIH-PA Author Manuscript

NIH-PA Author Manuscript

NIH-PA Author Manuscript

NIH-PA Author Manuscript

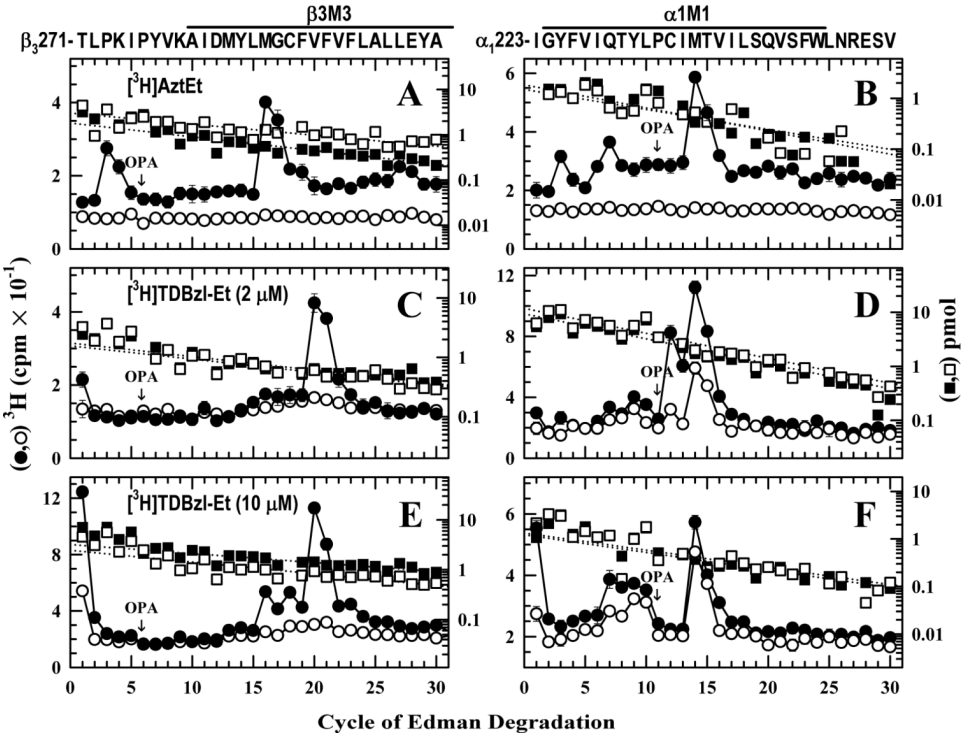

FIGURE 6. [^{3}H]Azietomidate and [^{3}H]TDBzl-etomidate photolabel amino acids in β3M3 and α1M1

^{3}H (●,○) and PTH-amino acids (■,□) released during N-terminal sequencing of subunit fragments beginning near the N-terminus of βM3 (**A,C,E**) or αM1 (**B,D,F**) that were isolated by rpHPLC (Supplemental Figures S1 and S2) from EndoGlu-C digests of β3 subunits and from trypsin (**B**) or EndoLys-C (**D, F**) digests of α1 subunits. Aliquots of α1β3 $GABA_AR$ (130 pmol of muscimol sites in 2 mL) were equilibrated with 1 mM GABA and either 700 nM [^{3}H]azietomidate (**A**&**B**), 2 μM (**C**&**D**) or 10 μM (**E**&**F**) [^{3}H]TDBzl-etomidate, in the absence (●,■) or presence (○,□) or of 100 μM etomidate (Et) and photolabeled, and then samples containing mostly β3 or α1 subunits were isolated by SDS-PAGE. **A, C, & E**, During sequencing of the β3M3 samples, the sequencing filters were treated with OPA prior to cycle 6 (β3Pro-276), thereby insuring that after cycle 5, only the peptide beginning at β3Thr-271 was sequenced (I_0 (*-Et/+Et*), in pmol: **A**, *1.8/3.0*; **C**, *1.7/1.6*; **E**, *3.2/2.4)*. **A**, The peak of ^{3}H release in cycle 16 indicates [^{3}H]azietomidate photolabeling of β3Met-286 (85 cpm/pmol), >95% inhibitable by etomidate. **C & E**, The peaks of ^{3}H release in cycle 20 indicate [^{3}H]TDBzl-etomidate photolabeling of β3Val-290 at 83 and 100 cpm/pmol, respectively, with etomidate inhibiting photolabeling by >95%. In **E**, the additional peaks of ^{3}H release in cycles 16 and 18 indicate photolabeling of β3Met-286 (–/+Et, 34/< 6 cpm/pmol) and β3Cys-288 (–/+Et, 16 /14 cpm/pmol). **B, D, & F**, Sequence analyses of the α1M1 samples, with OPA treatment prior to cycle 11 (α1Pro-233). After the OPA treatment, only the peptide beginning at α1Ile-223 was sequenced (I_0(-Et/+Et), in pmol: **B**, *1.8/1.5*; **D**, *7.8/10*; **F**, *1.2/1.3)*. **B**, the peak of ^{3}H release in cycle 14 indicates [^{3}H]azietomidate photolabeling of α1Met-236 (130 cpm/pmol), which etomidate inhibited by >95%. **D & F**, the peaks of ^{3}H release in cycle 14 indicate [^{3}H]TDBzl-etomidate photolabeling of αMet-236 at 82 and 190 cpm/pmol, respectively, which was reduced to 32 and 135 cpm/pmol in the presence of etomidate. In **D**, the peak of ^{3}H release in cycle 12 indicates photolabeling of α1Cys-234 at 49 and 9 cpm/pmol in the absence or presence of etomidate.

NIH-PA Author Manuscript

NIH-PA Author Manuscript

NIH-PA Author Manuscript

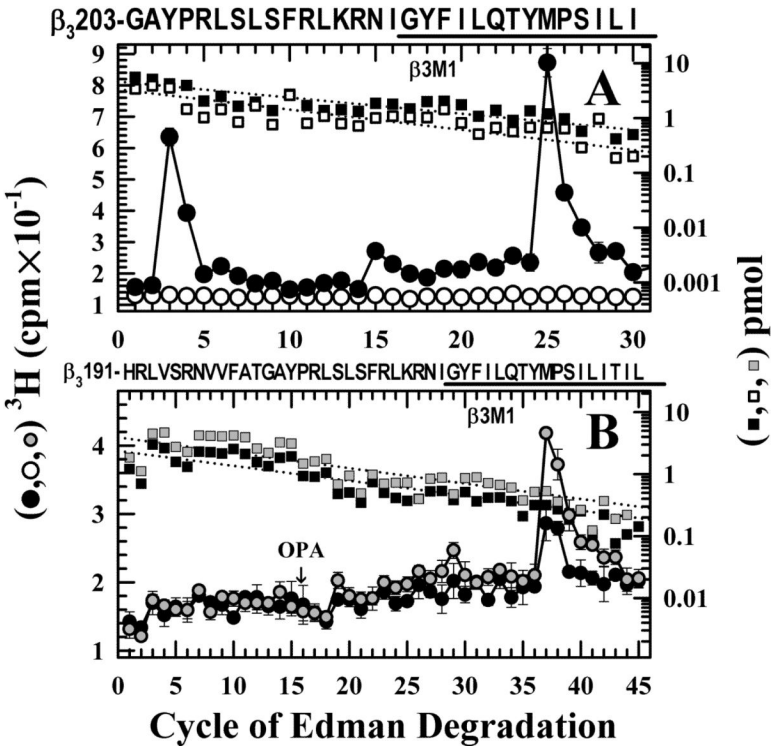

FIGURE 7. [^{3}H]Azietomidate photolabeling of β3Met-227 in βM1

^{3}H (●,○) and PTH-amino acids (■,□) released during N-terminal sequencing of subunit fragments beginning near the N-terminus of β3M1 that were isolated by rpHPLC (Supplemental Figures S1A) from EndoGlu-C digests of β3 subunits. Aliquots of α1β3 $GABA_AR$ were photolabeled with 700 nM [^{3}H]azietomidate in the presence of 1 mM GABA and in the absence (●,■) or presence (○,□) or of 100 μM etomidate (Et). **A**, the primary sequence began at β3Gly-203 (not an EndoGlu-C cleavage site, *I_0 (–/+Et) = 1.8/1.5 pmol)*, and the peak of ^{3}H release in cycle 25 indicated photolabeling of β3Met-227 in M1 at 150 cpm/pmol, which etomidate inhibited by >95%[2]. **B**, to confirm photolabeling of β3Met-227, a sample was sequenced from EndoGlu-C digests of β3 subunits from another photolabeling in the presence (black symbols) or absence (gray symbols) of GABA. This fragment began at β3His-191 (*I_0(+/–GABA) = 2.6/ 3.9 pmol*), a predicted EndoGlu-C cleavage site, and the sequencing filters were treated with OPA prior to cycle 16 (β3Pro-207). The peak of ^{3}H release in cycle 37 confirmed [^{3}H]azietomidate photolabeling of β3Met-227 (+GABA, 61 cpm/pmol; -GABA, 91 cpm/pmol).

NIH-PA Author Manuscript
NIH-PA Author Manuscript
NIH-PA Author Manuscript

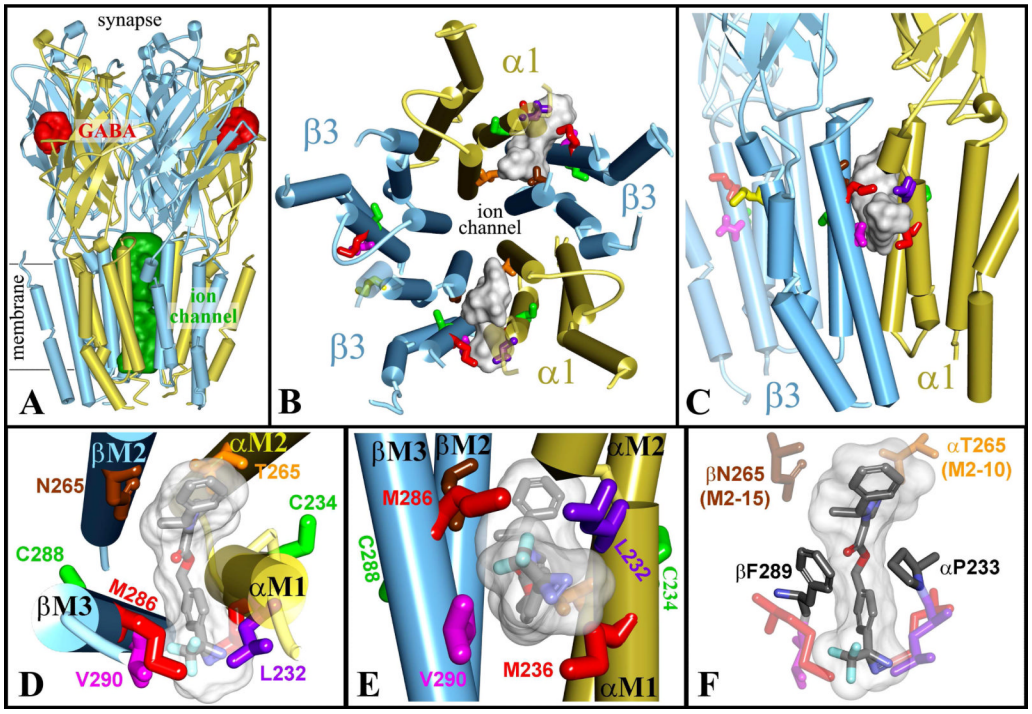

FIGURE 8. The binding sites for etomidate in the $GABA_AR$ transmembrane domain

A, a side view of an $(\alpha1)_2(\beta3)_3$ $GABA_AR$ homology model (α1, gold; β3, blue) based upon the structure of GLIC, the *Gloeobacter violaceus* proton-gated ion channel (PDB:3P50) (20). Connolly surface representations are included of the agonist binding sites (in red) in the extracellular domain and of the ion channel (green). **B & C**, views of the $GABA_AR$ transmembrane domain from the base of the extracellular domain (**B**) or from the lipid towards a β3-α1 interface (**C**), including Connolly surface representations of the volumes defined by the ensemble of the 100 lowest energy minimized TDBzl-etomidate docking solutions in the pocket at the β3-α1 interfaces (volumes, 720 and 820 $Å^3$). **D** & **E**, enlargements of the TDBzl-etomidate binding site shown in **B** & **C**, respectively, with the white transparent Connolly surfaces surrounding the 14 lowest energy TDBzl-etomidate docking orientations (volume, 510 $Å^3$). TDBzl-etomidate in its lowest energy orientation is included in stick format, color coded as to atom type: gray, carbon; red, oxygen; blue, nitrogen; and cyan, fluorine. In **B-E**, the amino acids photolabeled by [^{3}H]TDBzl-etomidate and/or [^{3}H]azietomidate are indicated in stick format with color coding (yellow, β3Met-227; red, β3Met-286 and α1Met-236; magenta, β3Val-290; green, α1Cys-234 and β3Cys-288). Also included in stick format are β3Asn-265 (βM2-15, brown), an etomidate sensitivity determinant (9,10), α1Leu-232 (in purple), a volatile anesthetic sensitivity determinant (1,33), and α1Thr-265 (M2-10), a position in the *Torpedo* nicotinic acetylcholine receptor α subunit photolabeled by [^{3}H]TDBzl-etomidate (23). **F**, a view of the β3-α1 binding site from the same perspective as **D**, but with the Connolly surface for TDBzl-etomidate in its lowest energy orientation and including two additional amino acid residues which must have extensive contact with the bound ligand: β3Phe-289 and α1Pro-233. The diazirine carbon is predicted to be within 5 Å of β3Met-286, β3Val-290, α1Leu-232, and α1Met-236; the N of β3Asn-265 and the O of α1Thr-265 are ~3 Å from the CH_3 carbon and the imidazole N-3, respectively.

NIH-PA Author Manuscript NIH-PA Author Manuscript NIH-PA Author Manuscript

Table 1

Pharmacological specificity of [^{3}H]azietomidate and [^{3}H]TDBzl-etomidate photoincorporation into residues in the α1β3 $GABA_AR$ (cpm/pmol of PTH-derivative)[a]

	[^{3}H]Azietomidate		[^{3}H]TDBzl-etomidate			
			2 μM		10 μM	
	-Etomidate cpm/pmol	+Etomidate *%inhibition*	-Etomidate cpm/pmol	+Etomidate %inhibition	-Etomidate cpm/pmol	+Etomidate *%inhibition*
αM1						
α1Cys-234	<5	*NQ*	55 ± 6	*80 ± 2 %*	28 ± 18	*<20 %*
α1Met-236	165 ± 35	*95 %*	90 ± 10	*56 ± 4 %*	160 ± 30 (n = 4)	*32 ± 8 % (n = 3)*
βM3						
β3Met-286	90 ± 5	*95 %*	8 ± 4	*65 ± 5 %*	32 ± 9 (n = 5)	*64 ± 20 % (n = 4)*
β3Cys-288	<6	*NQ*	7 ± 5	*-20 ± 30%*	30 ± 17 (n = 5)	*-10 ± 4 % (n = 4)*
β3Val-290	<6	*NQ*	80 ± 10	*97 ± 2 %*	90 ± 50 (n = 5)	*93 ± 4 % (n = 4)*
βM1						
β3Met-227	100 ± 45	*>95 %*	ND	*ND*	43 ± 20	*36 ± 6 %*

[a] ^{3}H incorporation (cpm/pmol of PTH derivative) in each residue was calculated from the observed ^{3}H release and the initial and repetitive yields as described under “Experimental Procedures”. When more than two samples were sequenced, the number, n, is indicated, and the values are mean ± SD. When two samples were sequenced, data are presented as mean (± range). The cpm/pmol are the values for positions at which the peak of ^{3}H release was ± 20 % over the background release in the previous cycles. The upper limits of the photolabeling in the other cycles were determined from the random variation of the background release of ^{3}H in the adjacent sequencing cycles. For samples photolabeled in the presence of etomidate, the % inhibition was calculated at each position as the ratio of cpm/pmol determined in the presence and absence of etomidate for the paired samples (i.e same rpHPLC fractions from a digest), and the means (±SD or range) are tabulated. ND, not determined; NQ, not quantified.

Biochemistry. Author manuscript; available in PMC 2013 January 31.